8-2012

Did Mineral Surface Chemistry and Toxicity Contribute to Evolution of Microbial Extracellular Polymeric Substances?

Jie Xu

Jay M. Campbell

Nianli Zhang

William J. Hickey

Nita Sahai
University of Akron Main Campus, sahai@uakron.edu

ASTROBIOLOGY
Volume 12, Number 8, 2012

DOI: 10.1089/ast.2011.0776

Did Mineral Surface Chemistry and Toxicity Contribute to Evolution of Microbial Extracellular Polymeric Substances?

Jie Xu,[1,2] Jay M. Campbell,[3] Nianli Zhang,[4,5] William J. Hickey,[6] and Nita Sahai[1,4,7,8]

Abstract

Modern ecological niches are teeming with an astonishing diversity of microbial life in biofilms closely associated with mineral surfaces, which highlights the remarkable success of microorganisms in conquering the challenges and capitalizing on the benefits presented by the mineral–water interface. Biofilm formation capability likely evolved on early Earth because biofilms provide crucial cell survival functions. The potential toxicity of mineral surfaces toward cells and the complexities of the mineral–water–cell interface in determining the toxicity mechanisms, however, have not been fully appreciated. Here, we report a previously unrecognized role for extracellular polymeric substances (EPS), which form biofilms in shielding cells against the toxicity of mineral surfaces. Using colony plating and LIVE/DEAD staining methods in oxide suspensions versus oxide-free controls, we found greater viability of wild-type, EPS-producing strains of *Pseudomonas aeruginosa* PAO1 compared to their isogenic knockout mutant with defective biofilm-producing capacity. Oxide toxicity was specific to its surface charge and particle size. High resolution transmission electron microscopy (HRTEM) images and assays for highly reactive oxygen species (hROS) on mineral surfaces suggested that EPS shield via both physical and chemical mechanisms. Intriguingly, qualitative as well as quantitative measures of EPS production showed that toxic minerals induced EPS production in bacteria. By determining the specific toxicity mechanisms, we provide insight into the potential impact of mineral surfaces in promoting increased complexity of cell surfaces, including EPS and biofilm formation, on early Earth. Key Words: Mineral toxicity—Bacteria—EPS evolution—Biofilms—Cytotoxicity—Silica—Anatase—Alumina. Astrobiology 12, 785–798.

1. Introduction

The mineral–water interface is a dynamic system in which multiple reactions, such as adsorption, dissolution–precipitation, redox, and photocatalysis, can occur depending on the specific mineralogy, surface chemistry, and environmental conditions (Banfield and Hamers, 1997; Brown *et al.*, 1999). These interfacial processes present a complex risk–benefit system for microorganisms in modern environments and, likely, during all stages of biogeochemical evolution on Earth. A mineral's beneficial, destructive, or lack of impact on cells depends on its surface chemistry and interactions with biomolecules or cellular components.

On the beneficial side, many nutrients are mobilized from minerals by dissolution, and interfacial redox reactions provide metabolic energy for diverse microorganisms (Nealson *et al.*, 1988; VanCappellen and Wang, 1996; Tebo *et al.*, 2004; Weber *et al.*, 2006). Sulfides, zeolites, weathered feldspars, and clays may have facilitated prebiotic chemistry and the origin of life by physically sheltering organic molecules in voids from UV radiation, concentrating organic species via adsorption and catalyzing RNA polymerization (Cairns-Smith, 1982; Wachtershauser, 1988; Ferris *et al.*, 1996). In contrast, minerals containing transition metals such as pyrite, olivine, and pyroxene catalyze nucleic acid degradation via surface free radicals generated by crushing or UV radiation (Schoonen *et al.*, 2006), and some oxides promote rupture of lipid vesicles (models for protocells) (Xu *et al.*, 2009).

Microbial communities may have evolved a survival strategy for life on rocks by converging upon a cooperative mode of existence enabled by a cohesive biofilm matrix. The biofilm comprises primarily extracellular polymeric

[1]Department of Geoscience and NASA Astrobiology Institute, [3]Department of Biochemistry, [4]Materials Science Program, University of Wisconsin, Madison, Wisconsin.
[2]Department of Chemistry, George Washington University, Washington, DC.
[5]Department of Biologic and Materials Science, School of Dentistry, University of Michigan, Ann Arbor, Michigan.
[6]Department of Soil Science, University of Wisconsin, Madison, Wisconsin.
[7]Environmental Chemistry and Technology Program, University of Wisconsin, Madison, Wisconsin.
[8]Department of Polymer Science and NASA Astrobiology Institute, University of Akron, Akron, Ohio.

substances (EPS), water, metabolites, cells, and cellular debris. The biofilm-forming cell aggregates may be either planktonic or attached to surfaces (Beveridge *et al.,* 1997; Hall-Stoodley *et al.,* 2004). EPS generation (predominantly polysaccharides, some proteins, and DNA) is usually controlled by an intricate feedback system of regulators and environmental cues, including nutrient availability and osmolarity (O'toole *et al.,* 2000; Sutherland, 2001; Stanley and Lazazzera, 2004).

The various functions of EPS have been exquisitely scrutinized in previous studies, including mediating cell attachment to surfaces and metabolic interactions between cells and minerals, quorum signaling, and lateral gene transfer (Costerton *et al.,* 1995; Miller and Bassler, 2001), and protecting against environmental extremes such as desiccation, nutrient depletion, temperature and pH fluctuations, and exposure to UV radiation or to soluble, toxic metals (Geesey *et al.,* 1988; Harrison *et al.,* 2007). In addition to the toxicity of soluble ions, the lethal dose of nanoparticles on planktonic bacteria at some single exposure period (Brayner *et al.,* 2006; Gogniat *et al.,* 2006) has also been determined by environmental toxicologists, and this is a burgeoning area, as novel synthetic nanoparticles are being developed for a myriad of medical, technological, and industrial applications (Nel *et al.,* 2009; Verma and Stellacci, 2010). As nanominerals and mineral nanoparticles are common and widely distributed throughout the atmosphere, oceans, groundwater, surface waters, and soils, as well as in and/or on most living organisms (Hochella *et al.,* 2008), these studies on toxicity of synthetic nanoparticles also have implications for our understanding of bacteria–mineral interactions in the earth system.

Some important basic questions regarding bacteria/EPS–mineral interactions, however, remain unexplored. Specifically, the potential role of EPS in shielding against mineral surface reactivity, the temporal response of cell viability to mineral exposure, and the possibility of toxicity-induced EPS production have not been systematically studied. Furthermore, a more nuanced picture of the specificity of mineral–water surface chemistry in determining cytotoxicity is required, rather than broad statements about minerals generically providing benign havens or acting as destructive agents toward prebiotic organic molecules, protocells, or the earliest cells on Proterozoic Earth.

We examined the cytotoxicity of model minerals (amorphous silica, SiO_2; anatase, β-TiO_2; and alumina, γ-Al_2O_3) toward two isogenic (of the same genotype) strains of a model microorganism, *Pseudomonas aeruginosa*. The PAO1 wild type is a copious biofilm-maker, whereas the Δ^-*psl* knockout mutant (Overhage *et al.,* 2005) has limited biofilm-forming ability. We also studied their EPS-removed counterparts (rPAO1 and rΔ^-*psl*) to ensure total absence of EPS in the initial state, and by comparing results of PAO1 vs. rPAO1 and Δ^-*psl* vs. rΔ^-*psl*, we can exclude the potential effects of *psl* deletion on other physiological functions that affect cell viability. The oxides chosen represent a range of surface reactivities (Table 1) and are insoluble at circumneutral pH, and oxyhydroxides are ubiquitous in the environment. We use the word "mineral" *sensu lato* to include both naturally occurring crystalline inorganic solid phases as well as amorphous inorganic phases. Ideally, one would use a single-locus mutant that is totally devoid of EPS, but to the best of our knowledge, such mutants have not been reported to date.

Using the Δ^-*psl* mutant is suitable to address the goals of this study because Δ^-*psl* cells do not produce certain exopolysaccharides that are critical in forming biofilms in natural environments. We showed that EPS shielded against mineral cytotoxicity, EPS production was induced by mineral exposure, cellular response varied with exposure time, and toxicity mechanisms were mineral-specific, and we considered the potential role of mineral cytotoxicity in the evolution of cell surfaces. To further illustrate how the study was carried out, we summarized the experimental design in Schematic 1.

2. Materials and Methods

2.1. Reagents and chemicals

All solutions used in the experiments were prepared with ultra-pure water (18.2 MΩ·cm) (Nanopore UV; Barnstead, Dubuque, IA). Fluorescent probes 3′-(p-aminophenyl) fluorescein (APF), 4′,6-diamidino-2-phenylindole (DAPI),

Table 1. Physiochemical Properties of the Oxide Particles and *Pseudomonas aeruginosa* Cells, and Reactive Oxygen Species Formation at the Oxide Particle Surfaces

	Particle Size[a] (nm)	Specific Surface Area[b] (m^2g^{-1})	PZC[c]	Ψ^d in H_2O (mV)	Ψ^d in 0.85% NaCl Saline (mV)	Ψ^d in cell culture solutions (mV)	Band Gap Energy[e] (eV)	[•OH] and [H_2O_2] (nM) in particle/DI water suspensions[f]
Silica	50, 275	47.18	1.8	−23.1	−15.4	−29.8	8.9	4.7, 401
Anatase	50, 241	8.79	4.8	−25.3	−19.1	−21.8	3.2	158, 1319
γ-Alumina	43, 270	26.91	7.8	46.5	49.5	−36.7	9.5	1.3, 434
PAO1 cell		–	–	–	−17.3	−11.7		
Δ *psi* cell		–	–	–	−19.9	−13.8		

[a]Primary particle size (left) reported by the manufacturer and confirmed here by transmission electron microscopy characterization, and secondary particle size (right) in ultrapure water (18 MΩ · cm resistivity at 25°C) suspensions. The secondary particle sizes were Z-averages calculated based on intensity-size distribution charts by dynamic light scattering, this study.
[b]Measured using N_2 multi-point BET adsorption isotherms, this study.
[c]Point of zero charge, cited from Sverjensky (1994) (Sverjensky D.A., 1994, *Geochimica et Cosmochimica Acta*, 58, 3123–3129).
[d]Zeta-potential, this study.
[e]Cited from Xu and Schoonen (2000) (Xu Y., Schoonen, M.A.A., 2000, *American Mineralogy,* 85, 543–556).
[f]Measured using the APF probe, this study.

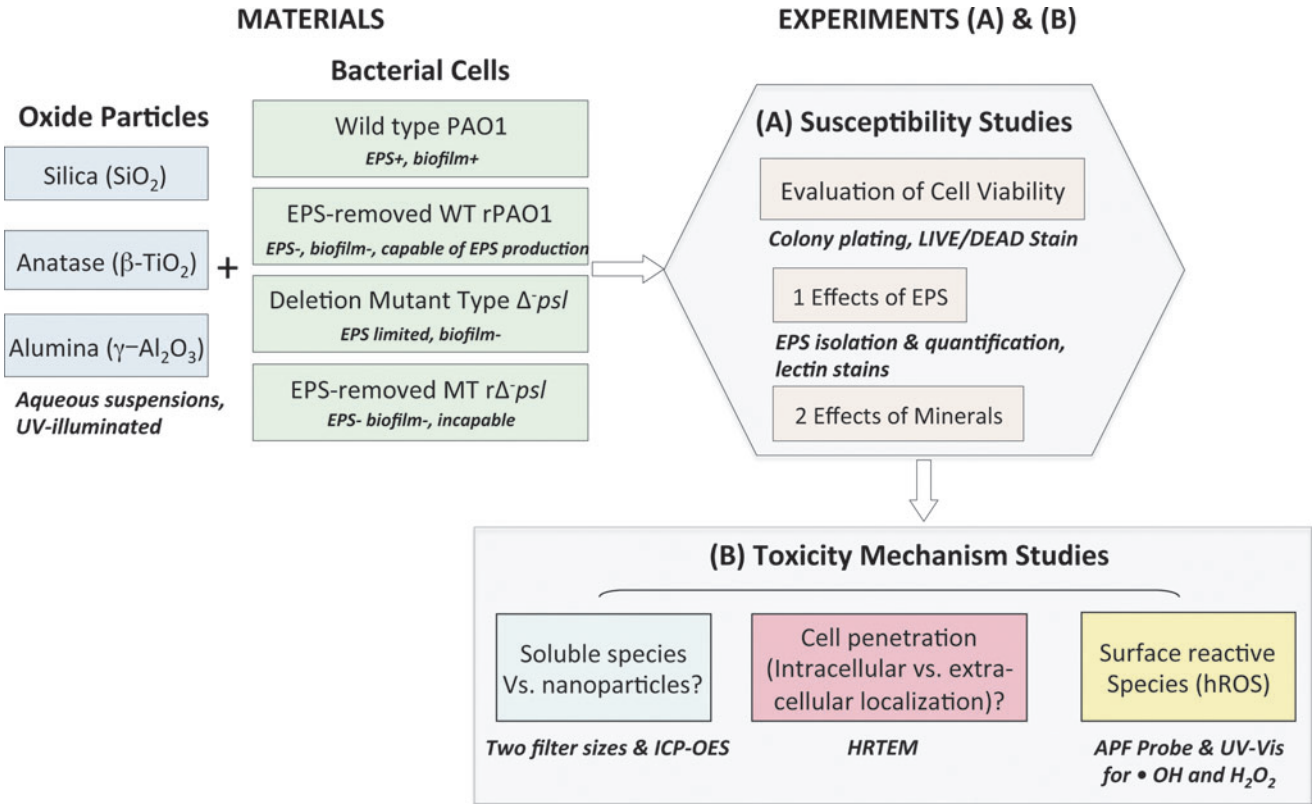

SCHEMATIC 1. Summary of experiments. (Table 3S provides information on culture media used.)

fluorescein isothiocyanate-conjugated concanavalin-A (conA-FITC), tetramethyl rhodamine isothiocyanate-conjugated wheat germ agglutinins (WGA-TRITC), and the LIVE/DEAD Baclight® kit were purchased from Invitrogen (Carlsbad, CA). Luria-Bertani (LB) broth and ultra-pure agar powders were purchased from MP Biomedicals (Carson, CA). All other chemicals and solvents used were of American Chemical Society (ACS) grade and purchased from Sigma-Aldrich (St. Louis, MO).

2.2. Preparation and characterization of oxide suspensions

Powders of amorphous silica (Degussa), anatase, and γ-alumina (Sigma-Aldric) were cleaned prior to use by dialysis against ultra-pure water (18.2 MΩ·cm) for ~3 days. Chemical compositions of the commercial oxides were confirmed by the chemical analysis conducted by ALS Chemex Laboratory (Reno, NV), and crystalline structures of the oxides were confirmed by X-ray diffraction patterns. Specific surface area was measured for each oxide by using a multipoint, N_2 BET adsorption isotherm (Quantachrome Intruments, Boynton Beach, FL). Oxide suspensions in water for the susceptibility tests were prepared by adding 10 mg of autoclaved oxide powders into 10 mL sterile ultra-pure water. The suspension was subsequently sonicated for 2 hours to disperse the particle aggregates and exposed to UV illumination at 254 nm (8 Watt) for 2 h to investigate the ability of the oxides to generate highly Reactive Oxygen Species (hROS), which are capable of lysing cells by oxidizing phospholipid cell membranes. These tubes were shaken and vortexed once ~every half hour during the UV-illumination. Surface charge and size distribution of the dispersed and illuminated particles were determined by Dynamic Light Scattering with a Malvern NanoZetasizer (Malvern Instruments, United Kingdom).

2.3. Bacterial strains and growth conditions

The *Pseudomonas aeruginosa* strains PAO1 and Δ-*psl* used in this study were generously provided by Professor M. Parsek (University of Washington, Seattle, WA) and Professor Y. Liu (University of Wisconsin, Milwaukee, WI). Lyophilized cells were restored and grown in LB broth for ~ 24 h. The cell culture was then mixed with sterile glycerol at a 1:1 (v:v) ratio. The mixture was aseptically distributed in 1 mL aliquots and stored at −80°C. For each susceptibility experiment, one aliquot of the previously prepared stock was transferred into a sterile 250-mL Erlenmeyer flask containing 50 mL of fresh LB broth, and the culture was grown at 30°C on a rotary shaker (150 rpm) for ~30 h before harvesting for the susceptibility tests.

2.4. Susceptibility tests

Cell cultures for the susceptibility tests were harvested at their mid-exponential growth phase (Fig. 1S; Supplementary Material available online at www.liebertonline.com/ast) and prepared in two different ways: (1) no treatment, and (2) centrifuged (2000 g, 10 min, room temperature), the supernatant removed, and the cells washed and resuspended in fresh 0.5% (wt) saline solution. We refer to (1) and (2),

respectively, as original PAO1 for the wild type and $\Delta^{-}psl$ for the mutant, and washed rPAO1 for the wild type and $r\Delta^{-}psl$ for the mutant cell cultures. The impact of the washing step on cell viabilities was evaluated by LIVE/DEAD® assays and found to be minimal.

Cell susceptibility to the suspended oxide particles was determined in liquid media, where 4 mL of each type of cell culture was mixed with an equal volume of each oxide suspension in a 15 mL centrifuge tube and incubated on a rotary shaker (100 rpm) at 30°C for up to 8 h. For each cell–oxide sample, an oxide-free cell control was prepared identically, except that deionized (DI) water replaced the oxide particle suspensions. Duplicate samples were prepared for each cell–oxide combination, and triplicate samplings were conducted at each time point for each sample. Culturable bacterial cells in the control or oxide samples were assayed by plating on LB–agar plates following serial dilutions in 0.5% (wt) saline solution. And the colony forming units (CFU) on agar plates were counted and used for evaluation of cell viabilities. Duplicate plates were prepared for each sampling, and thus, each data point was an average of 9–12 analyses. The entire experiment was repeated twice.

To evaluate the effect of oxide particles on cell growth, while accounting for the variations in the initial cell viability among and between experiments, we defined a novel "mineral impact index" (χ) to account as:

$$\chi = \frac{(CFU_{control,t} - CFU_{mineral,t})}{(CFU_{control,t} - CFU_{control,t=0})} \times 100\%$$

(Note: $CFU_{control,\ t} > CFU_{control,\ t=0}$ throughout the experiments.)
$\chi \leq 0$, the oxide has no effect. $0 \leq \chi \leq 1$, the oxide is bacteriostatic. $\chi \geq 1$, the mineral shows bacteriocidal effect.

2.5. LIVE/DEAD Assay

Stock solutions of two nucleic acid stains, the green-fluorescent SYTO®9 stain and the red-fluorescent propidium iodide stain, were mixed at a 1:1 ratio. The mixture was then added to 1000 μL of the diluted samples (diluted $\times 10$ with 0.5% NaCl) at a 1:100 ratio. SYTO®9 labels both live and dead cells, while propidium iodide can only penetrate cells with damaged membranes, which reduces SYTO®9 fluorescence when both dyes are present. Thus, under the epifluorescence microscope, live cells with intact membranes fluoresce green, and dead cells with damaged membranes fluoresce red. After incubation in the dark for 15 min at room temperature, 100 μL of each stained sample was filtered through a 0.2-μm-sized polycarbonate membrane (Whatman, Piscataway, NJ). The membrane was subsequently removed onto a clean glass slide, mounted with mineral oil, covered with glass slips, and imaged by a Nikon Eclipse 90i microscope (Nikon Instruments, Tokyo, Japan). Two slides were prepared for each sample, and at least 10 locations were examined for each slide.

2.6. Inductively coupled plasma—optical emission spectrometry

Solutions from the oxide susceptibility tests were collected at each time point to determine the concentrations of dissolved Si, Ti, and Al (soluble metals). One mL of each sample solution was taken at each time point and centrifuged at 12,000 rpm for 5 min to remove heavy solids, and the supernatants were filtered through either 0.2-μm-sized polyvinylidene fluoride filters or 100 kD centrifugal filters. The filtered solutions were analyzed by optical emission spectrometry (ICP-OES) (Varian Vista-MPX, Varian Australia). Duplicate samples were prepared for each cell–oxide combination, and triplicate samplings were conducted at each time point for each sample. Each data point was an average of six analyses. The entire set of experiments was repeated twice.

2.7. Detection and quantification of H_2O_2 and OH radicals in the oxide suspensions

A fluorescent probe, 3′-(*p*-aminophenyl) fluorescein (APF), was used for the detection of hROS present in the oxide suspensions. The method has been described previously in detail (Cohn *et al.,* 2009). A calibration curve was generated by incubating known amounts of H_2O_2 with 10-μM APF, 50 mM potassium phosphate buffer of pH 6.0, and 2.95 units$\cdot$mL^{-1} type-II HRP (Sigma-Aldrich) in 2 mL centrifuge tubes placed on a Labquake® tube rotator (Thermo Fisher Scientific, Waltham, MA) in the dark at room temperature. After 24 h, the solutions were transferred to methalcrylate cuvettes with four clear sides for fluorescence measurements by a PC1 spectrofluorometer (ISS, Champaign, IL) with excitation and emission wavelengths set to 490 nm and 515 nm, respectively. This measure yields a linear correlation between the fluorescence data and the generated [•OH] (H_2O_2 were transformed to •OH in the presence of HRP). Using the calibration curve generated in this way, we examined the oxide suspensions with various particle loadings both without HRP and with HRP, because H_2O_2 can only be detected in the presence of HRP. The difference between analyses with and without HRP provides information of the generated [H_2O_2]. Triplicates were prepared and examined for each oxide sample. The entire experiment was repeated twice.

2.8. Lectin stains for EPS visualization

Fluorescein isothiocyanate-conjugated *Canavalia ensiformis* (conA-FITC) and tetramethyl rhodamine isothiocyanate-conjugated *Triticum vulgaris* (WGA-TRITC) were used in combination with 4′,6-diamidino-2-phenylindole (DAPI) to examine the presence of polysaccharides at the surfaces of PAO1, rPAO1, and $r\Delta^{-}psl$ cells. Lectins (i.e., conA and WGA) bind specifically to carbohydrates, whereas DAPI binds specifically to cell DNA. Using lectins and DAPI simultaneously can provide good information on EPS distribution versus cell distribution. Carbohydrate binding specificity of the two lectins has also been proposed and evaluated previously, where conA-FITC binds to mannose and glucose, and WGA-TRITC binds to N-acetylgalactosamine residues and oligomers, N-acetylneuraminic acid, and N-acetylmuraminic acid (Neu *et al.,* 2001). Working solutions consisting of 100 μg$\cdot$mL^{-1} of each stain were prepared with sterile phosphate buffered saline (PBS) and stored at −20°C until further uses. One mL of each sample for examination was centrifuged at 12,000 g for 15 min. Pelleted cells or cell–particle mixture were covered by 15μL of the stain solution on a glass slide and incubated in the dark at room temperature for 20 min. Excess stain on the slide was removed by rinsing gently with PBS.

Signals of FITC, TRITC, and DAPI were detected and analyzed at different excitation/emission wavelengths (488/518 nm for FITC, 550/570 nm TRITC, and 350/450 nm for DAPI) by an epifluorescence microscope (Eclipse 90i, Nikon Instruments). For each sample, at least 10 areas were examined, and the displayed micrographs are representative of the samples.

2.9. Extraction and quantification of the EPS production

We extracted free and capsular EPS, respectively, from the susceptibility samples and subsequently quantified them to track the production of EPS over time in different systems. The protocol used for EPS isolation was modified from previously described methods (Omoike and Chorover, 2004; Metzger *et al.*, 2009). Cells from the oxide susceptibility samples and oxide-free controls were harvested by centrifugation at 12,000 g for 15 min at 4°C. The cell pellets (~10–15 mg wet weight) were used for extraction of the capsular EPS, and the supernatant was used for extraction of the free EPS. The cell pellets were resuspended in 1 mL of 0.5% (wt) NaCl solution to obtain a biomass concentration of $\sim 10\,mg \cdot mL^{-1}$ and homogenized for 30 min on an icepack (~4°C) by using a Wheaton homogenizer tube and pestle. Formaldehyde (37%) was added at a 1:100 (v:v) ratio to the homogenized samples, and after 2 h, 1N NaOH was added at a 1:10 (v:v) ratio. The mixture was maintained at 4°C for 2 h and centrifuged at 12,000 g for 15 min. The supernatant was filtered (polyvinylidene difluoride [PVDF] membrane, pore size 0.45μm; Millipore, Billerica, MA), dialyzed against ultrapure water for 20 h at 25°C with 3500-molecular-weight-cutoff (MWCO) Spectra/Por® dialysis tubings, and collected for lyophilization.

The supernatant separated from each centrifuged oxide susceptibility sample or oxide-free control was precipitated with 3× volume of ethanol and stored at −20°C for 20 h. The precipitates were then removed by centrifugation (20,000 g, 15 min at 4°C) and resuspended in 500 μL ultra-pure water followed by dialysis with 3500 MWCO Spectra/Por® dialysis tubings.

The total carbohydrate content was measured by a modified phenol–sulfuric acid method with glucose standards. First, 500 μL of each EPS-containing solution was mixed with 1250 μL of sulphuric acid (>98%) and 250 μL of 10% phenol, and then the mixture was heated in a water bath at 98°C for 5 min. The mixture was cooled and measured for absorbance at 490 nm by an UV/Vis spectrophotometer (UV-mini 1240; Shimadzu Corp, Kyoto, Japan). The final results were normalized by the dry weight of the collected biomass. Duplicate samples were prepared for each cell–oxide combination, and triplicate aliquots were analyzed for the extracted EPS from each sample. The entire experiment was repeated twice.

2.10. High Resolution Transmission Electron Microscopy (HRTEM)

Samples were high pressure-frozen (Balzers HPM010, Widnau, Switzerland) and transferred to 2-mL cryovials containing 2% osmium tetroxide in acetone. Freeze substitution was carried out in a styrofoam cooler filled with dry ice for 95 hours, and then samples were transferred and stored in a −20°C freezer for 24 h. Subsequently, the sample temperature was allowed to rise slowly to 4°C over a 24 h period. The samples were rinsed three times with pure acetone and embedded in EmBed 812 resin (Electron Microscopy Sciences, Hatfield, PA) over a course of 2 days. The epoxy resin was cured at 65°C overnight and sectioned to a thickness of ~70 nm with a 55° Diatome diamond knife. Imaging was performed with a Tecnai T12 Transmission Electron Microscope (FEI Corp., Hillsboro, OR) at 80KV. Images were captured by a Gatan ES500W side-mounted charge-coupled device (CDD) camera with a resolution of 1350×1040 pixels. For each cell–oxide combination, duplicate samples were prepared and at least eight areas were examined for each sample. The displayed micrographs are representative of the corresponding samples.

3. Results

3.1. Mineral toxicity toward wild-type versus EPS-defective mutant cells

Cell viability was determined during exposure to oxide particle suspensions over a period of 8 h relative to the corresponding oxide-free controls (Figs. 1 and 1S). In general, the cell susceptibility to minerals increased as PAO1 < Δ⁻*psl* < rPAO1 < rΔ⁻*psl*. In detail, the PAO1 cell population declined upon initial exposure to the oxide particles, but recovered after a very short period of acclimation (Fig. 1a), whereas Δ⁻*psl* cells were slightly affected throughout the experiment period. The viability of rΔ⁻*psl* cells was significantly (Table 1S) lower in the presence of the oxide particles, especially anatase and alumina (Fig. 1b, c), and continued to remain low up to 8 h. The response of rPAO1 cells to the oxides differed from that of both PAO1 and rΔ⁻*psl*. After a sharp drop in relative viability, the rPAO1 cell population recovered to a similar level as the oxide-free controls.

3.2. Oxide-specific cytotoxicity

The oxides showed different degrees of cytotoxicity toward the EPS-depleted cells, increasing as amorphous silica < anatase < γ-alumina. To describe the specific mineral effect, we developed a novel mineral impact index, χ, to account for variations in the initial cell viability among and between experiments (Fig. 1d–f and Supplementary Material). The γ-alumina particles were bacteriocidal ($\chi > 1$) to the EPS-removed cells, and were distinguished from the anatase particles that were bacteriostatic ($0 < \chi < 1$) and amorphous silica, which showed minimal or no effect ($\chi < 0$). Cell viabilities estimated by epifluorescence microscopy and the LIVE/DEAD® assay (Fig. 2S) were consistent with the quantitative plating results.

3.3. EPS production

To determine the involvement of EPS in the cell–mineral interactions, qualitative lectin-binding analysis of EPS (Fig. 2) was conducted for centrifuged samples from the susceptibility tests. For the oxide-free controls, at t = 0, the PAO1 cells were well encapsulated by EPS as shown by the red and green fluorescent lectin stains, and formed biofilms as inferred from the cloudy appearance of the DAPI stain, indicating three-dimensional cell aggregates. The Δ⁻*psl*, rPAO1, and rΔ⁻*psl* cells were almost devoid of EPS capsules (Fig. 2, column 1). The EPS status of PAO1 and rΔ⁻*psl* persisted in

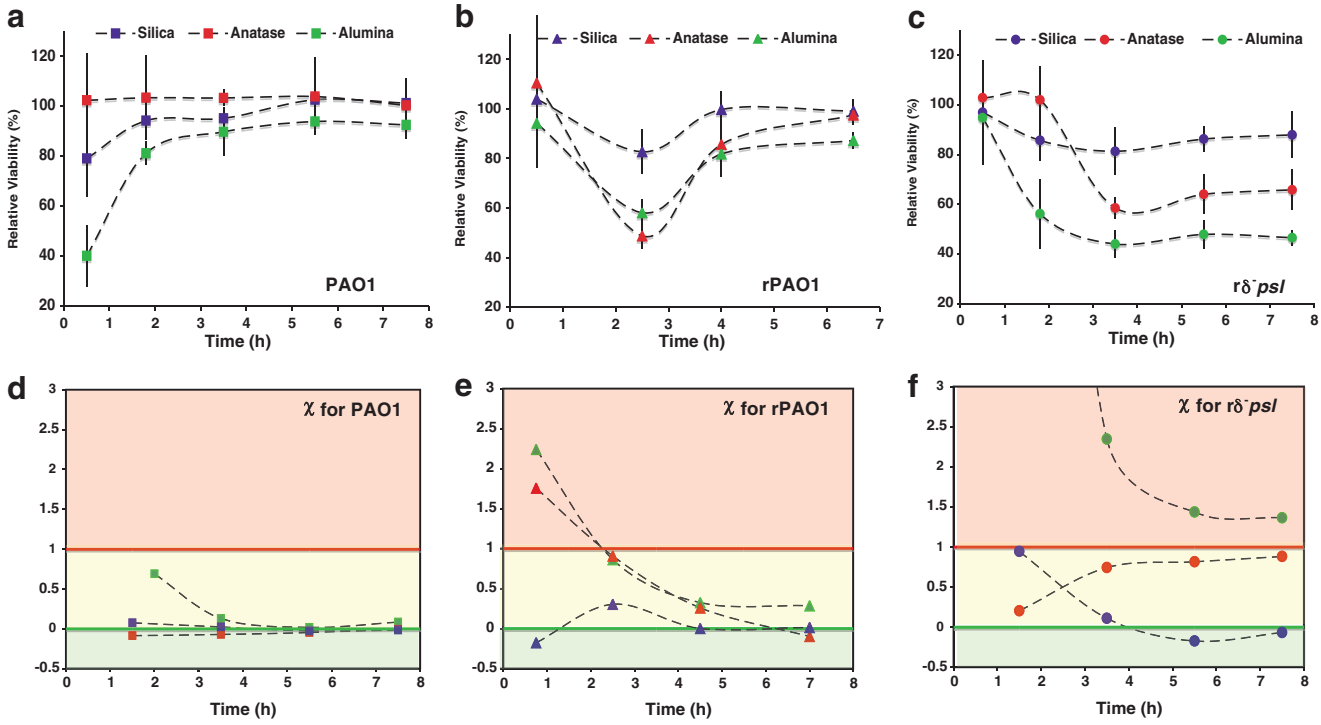

FIG. 1. Time profiles of relative cell viabilities in the susceptibility samples (**a–c**) obtained by plating and counting colony forming units (CFUs). Statistical significance tests were conducted for the results, and information is provided in the Supplementary Material (available online at www.liebertonline.com/ast). The susceptibility of the cell populations to the presence of oxide minerals varied with cell-type and with oxide-type (see text). The contrasts in cell response are highlighted by comparing (**a**) the PAO1 cells, which were susceptible in the first 15 minutes but recovered rapidly with (**c**) the rΔ^{-}*psl* cells, which were tolerant at 15 min, but the population declined thereafter. The mineral effect on the cells was quantitatively represented by a novel impact index, χ, defined in the box (below). Time profiles of χ values for the oxides on each cell type are shown, respectively, in (**d**)–(**f**). When $\chi \leq 0$, the oxide mineral has no effect on the bacterial cells (green zone); when $0 \leq \chi \leq 1$, the mineral shows bacteriostatic effect (yellow zone); and when $\chi \geq 1$, the mineral shows bacteriocidal effect (red zone).

the oxide-free controls up to 5 h, compared to both Δ^{-}*psl* and rPAO1 cells, which formed cell aggregates and generated detectable amounts of EPS in that time (Fig. 2, column 2). After 5 h exposure to oxide particles, the rΔ^{-}*psl* remained almost devoid of EPS, whereas PAO1, Δ^{-}*psl*, and rPAO1 cells demonstrated the presence of EPS capsules. Among the oxides, EPS-rich biofilms were formed in the presence of γ-alumina (Fig. 2, column 5) by all cell types except r Δ^{-}*psl*.

We also quantified the amount of (1) capsular EPS, which is associated closely with the cell surface and is crucial for biofilm formation, (2) free EPS, which is loosely associated with the cells and predominantly generated by sloughing off from capsular EPS, and (3) total EPS, focusing on PAO1, rPAO1, and rΔ^{-}*psl* cells (Fig. 3). The PAO1 solutions were extremely rich in free EPS throughout the experiments, and capsular EPS production was enhanced in the presence of the oxides. In oxide-free controls, rPAO1 and rΔ^{-}*psl* cells had very small amounts of capsular and free EPS at t = 0 compared to PAO1 cells. After 8 h exposure to oxides, however, rPAO1 cells formed capsular EPS of comparable quantity to PAO1 cells, while rΔ^{-}*psl* cells remained low in both capsular and free EPS. These results are consistent with the lectin-binding analyses above.

Capsular EPS generation in nutrient-limited (0.85% saline solution) conditions like the rPAO1 system was based on generic physical recognition of the particles without an oxide-specific effect. Oxide-specific capsular EPS production was obtained in nutrient-rich (LB medium) conditions like the PAO1 system with maximum capsular EPS formation in the presence of the most toxic mineral, γ-alumina, and the least EPS in the presence of the minimally toxic amorphous silica.

Comparing the susceptibility tests and EPS production results, we established a positive correlation between the presence of EPS and the bacterial resistance to oxide toxicity. This result provides support for our hypothesis that EPS shields against mineral toxicity.

3.4. Mineral properties potentially controlling oxide toxicity

3.4.1. Soluble metals versus nanoparticles. Both 0.2-μm PVDF filters and 100-kD centrifugal filters were used to remove particulate solids preceding soluble element analyses of sample solutions (see Methods section). Any difference in the "soluble" metal concentrations of the two filtrates would indicate that the detected species in the 0.2-μm-filtered samples were a combination of truly dissolved ions and of nanoparticles $< 0.2\,\mu$m. Amorphous silica solubility was low in DI water, but increased greatly in the presence of cells and EPS (Fig. 4A).

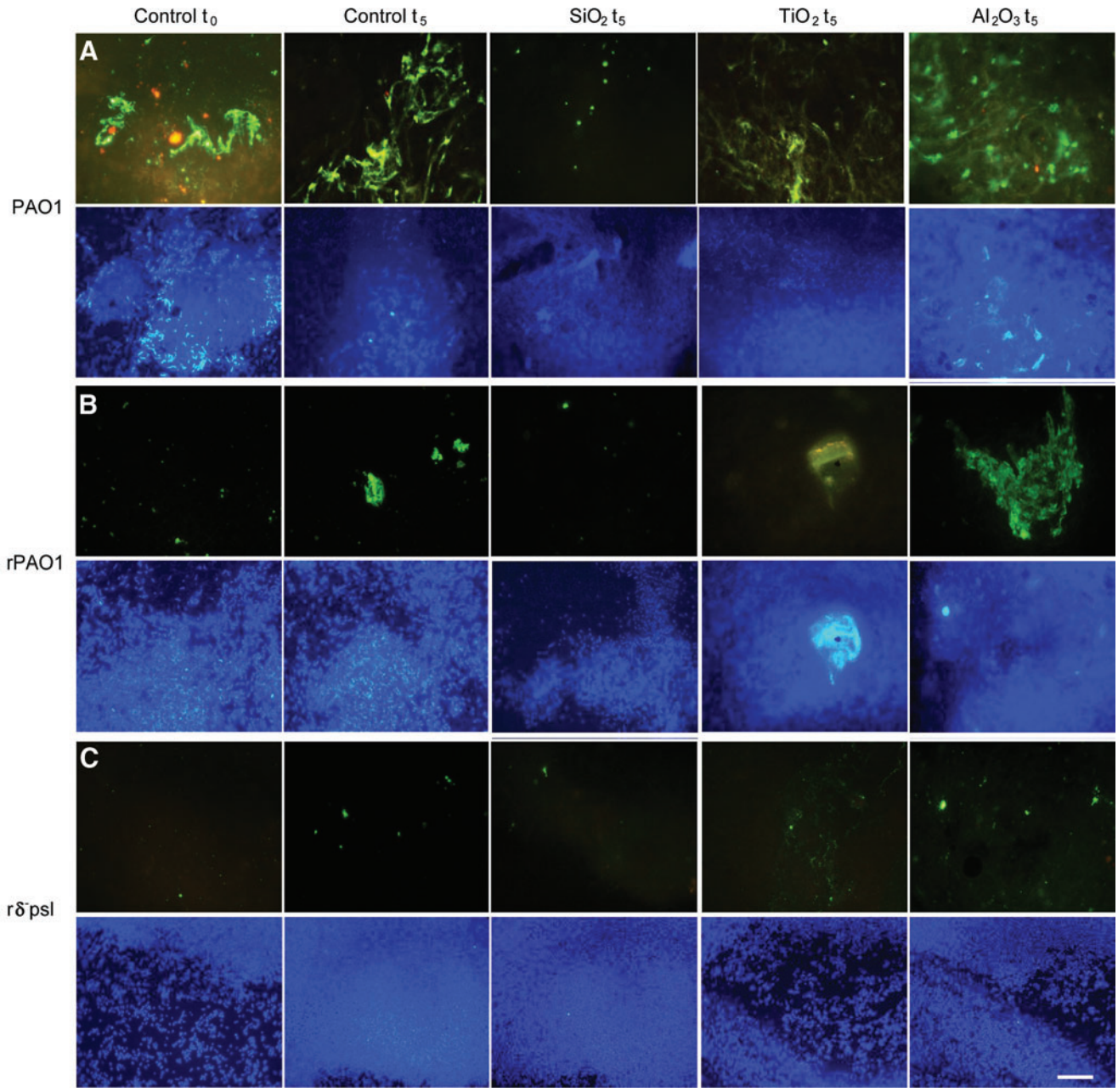

FIG. 2. Characterization of the effects of oxide particles on extracellular polymeric substances (EPS) production and biofilm formation compared to oxide-free controls (horizontal), for various cell types (vertical), in the centrifuged pellets of susceptibility samples. The EPS was characterized by two fluoro-conjugated lectins, wheat germ agglutinin (red signal) and concanavalin-A (green signal). A nucleic acid stain DAPI (purple signal) was employed simultaneously to visualize the corresponding cell distribution as cell aggregate–forming biofilms versus dispersed cells. **Columns 1–5**: oxide-free control at t = 0, control at t = 5 h, amorphous silica + cells at t = 5 h, anatase + cells at t = 5 h, and γ-alumina + cells at t = 5 h. **Row A-C**, PAO1, rPAO1, and rΔ^-*psl*. The indicated scale bar is 10 μm. Cell-free mineral controls were pre-tested with the lectin and DAPI stains and showed negligible background fluorescence. Presence of EPS was indicated by the green and red fluorescent areas. Biofilm formations were inferred from the cloudy, out-of-focus areas of the DAPI stain, suggesting three-dimensional cell aggregates (PAO1, Row A and rPAO1, Row D). For rΔ^-*psl*, the DAPI stain showed separated spots suggesting more dispersed, less aggregated cells and no biofilm (Row C).

Both anatase and γ-alumina particles were highly insoluble in DI water (pH 6) and cell culture solutions (pH 6–7.2). There was no change in Ti solubility based on filter size. In contrast, an apparent difference was observed in Al solubility based on filter size. Interestingly, a lower concentration of nano-sized γ-alumina was obtained from the rΔ^-*psl* culture medium filtrate compared to that from PAO1, which may suggest intracellular uptake by the rΔ^-*psl* cells.

3.4.2. Intracellular versus extracellular nanoparticles. Electron-dense spots are interpreted as oxide particles. No oxides were observed inside the PAO1 cells. Negatively

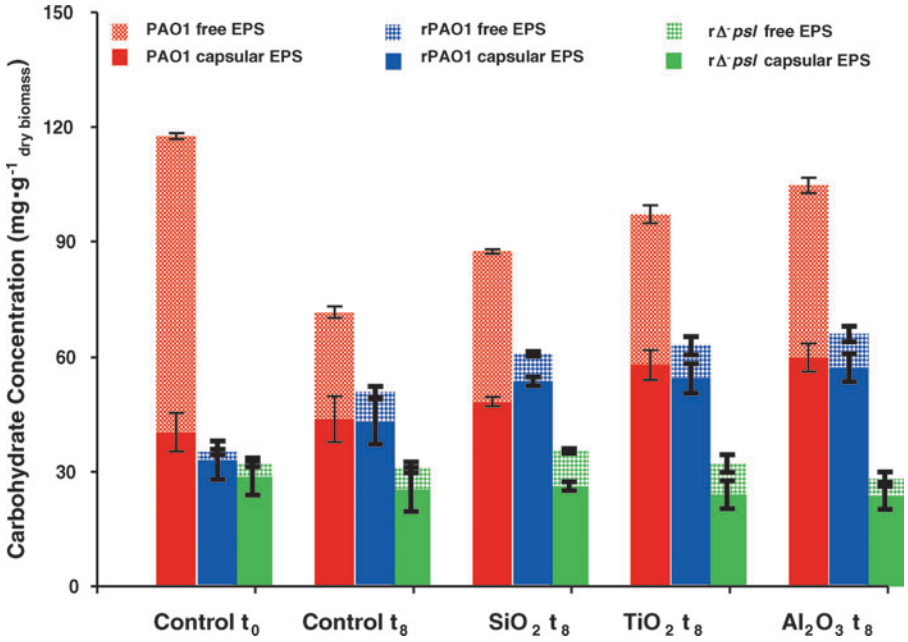

FIG. 3. Quantitative determination of the effects of oxide particles on free and capsular EPS production compared to oxide-free controls, for PAO1, rPAO1, and rΔ^-*psl*, in the susceptibility samples (see Supplementary Material). The results were normalized to the dry weight of biomass in each sample. Statistical significance tests were conducted for the results (see Supplementary Material). The high concentration of free EPS in the PAO1 control at t_0 was mainly attributed to the relatively low cell density at t_0.

charged amorphous silica and anatase particles were not observed within the rΔ^-*psl* cells (Fig. 5). Only γ-alumina particles were observed inside cells, and the internalized particles were < 50 nm in size. We did not observe any electron-dense areas inside the cells of the oxide-free controls, which indicates that the dark spots were not an artifact of the osmium tetroxide staining.

3.4.3. Surface charge. The bacterial cell surface, silica, and titania particles were negatively charged in all solutions (Table 1). The γ-alumina particle surfaces were positively charged in the rPAO1 and rΔ^-*psl* solutions, but the surface charge was reversed, becoming negative in the PAO1 solution (Table 1).

3.4.4. Surface-associated oxidative stress. High concentrations of H_2O_2 and •OH were detected in the particle/water suspensions of anatase but not of amorphous silica or alumina (Table 1). We also tested the susceptibility of rΔ^-*psl* cells to anatase with and without bovine liver catalase (see Methods), an enzyme that promotes scavenging of hROS to oxygen and water. The catalase-treated particles showed a much lower toxicity toward the cells (Fig. 6).

4. Discussion

4.1. Roles of EPS against oxide surface effects

The viability of wild-type cells and EPS-removed wild-type cells was, in general, higher than that of the EPS-free mutants, which suggests that EPS does protect against mineral toxicity. We interpret the early tolerance seen in the rPAO1 and rΔ^-*psl* cells to be a consequence of the EPS-removing procedure, which could have induced a defensive mode in the cells preceding exposure to the oxides. These cells were then able to cope with the presence of the particles in a shorter time. In contrast, the non-treated PAOI and Δ^-*psl* cells were stress-free until the oxide particles were introduced, so these cells took a longer time to adopt a defensive strategy against the minerals.

The results of the susceptibility and EPS production tests taken together showed a positive correlation between the presence of EPS and the bacterial resistance to oxide toxicity. The PAO1 cells, which produced abundant EPS and formed biofilm throughout the experiment, were barely affected by the oxide particles. In contrast, the rΔ^-*psl* cells, which produced minimal EPS and had limited biofilm-forming ability were the most susceptible to mineral toxicity. The rPAO1 cells started as devoid of EPS and were initially affected by the oxides, but the population recovered slowly when EPS formation was initiated in response to the oxide exposure. We speculate that EPS-supported cell aggregates created micro-zones that permitted localized nutrient recycling and heterogeneous cell growth, which led to eventual recovery of the rPAO1 cell population, even in nutrient-depleted conditions. The Δ^-*psl* cells showed behavior intermediate to PAO1 and rPAO1, as anticipated for a mutant that has retained some ability to generate EPS. Thus, EPS protected against mineral toxicity, and EPS production could be stimulated by exposure to minerals.

Nutrient availability in cell culture medium/suspension solution affected the production of free EPS versus capsular EPS in different ways. Free EPS production was controlled mainly by the nutrient availability in the culture/suspension medium, enriched for PAO1 in LB medium versus depleted for rPAO1 (0.85% saline solution), and was relatively insensitive to the presence or absence of oxide particles. Intriguingly, the production of capsular EPS could be induced by external stimuli such as oxide particles, and furthermore, the specificity of particle recognition depended on the culture/suspension solution. In detail, capsular EPS production in nutrient-limited (85% saline solution) was based on generic physical recognition of particles (e.g., rPAO1 system), but was oxide-specific in nutrient-rich LB medium (e.g., PAO1 system). Maximum capsular EPS was generated in the presence of the most-toxic oxide, γ-alumina, and minimal production was obtained for silica.

The mechanisms by which free versus capsular EPS provided protection against the nanoparticles were also

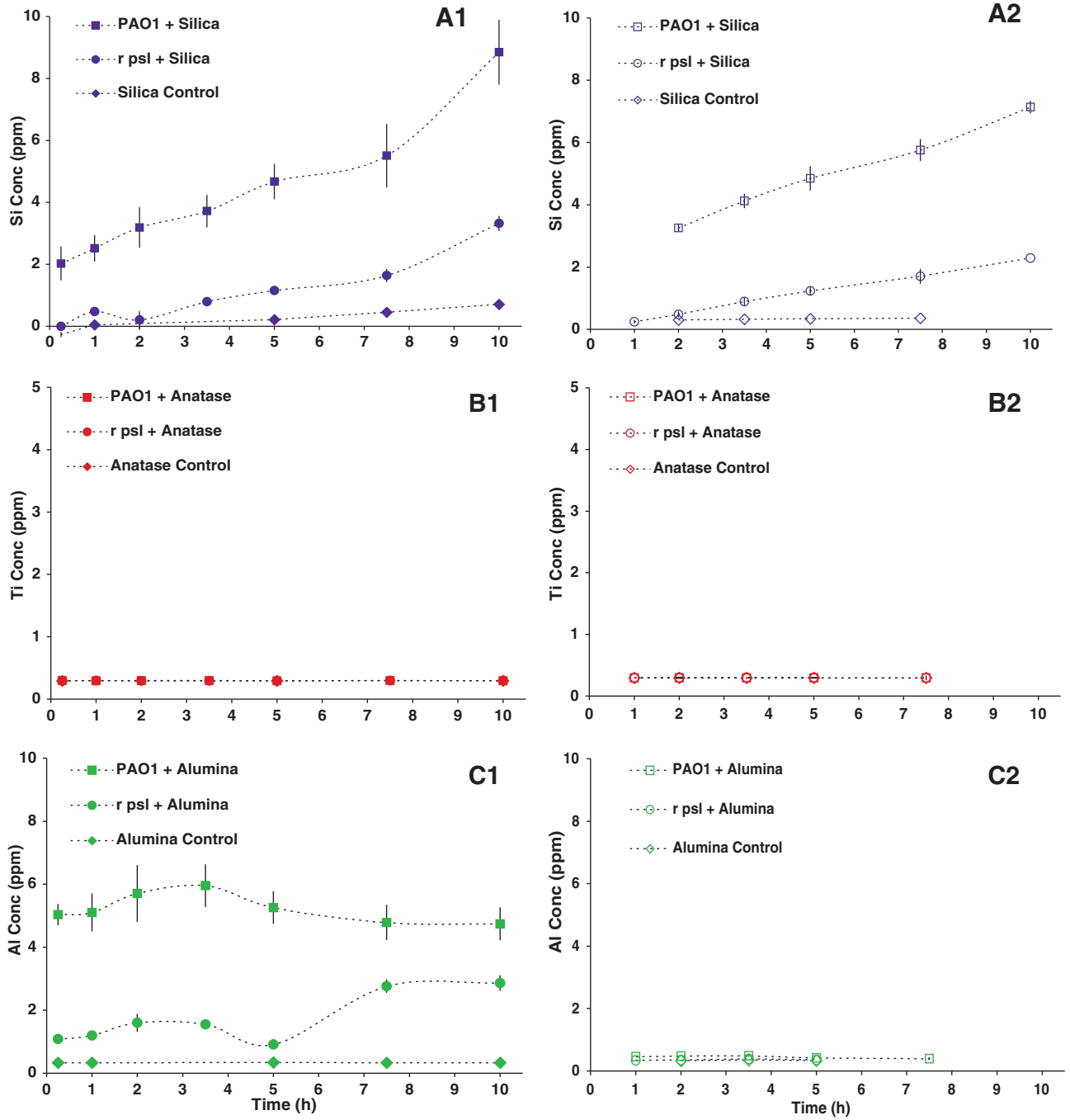

FIG. 4. Soluble Si, Ti, and Al concentrations over the time period of the oxide-susceptibility tests (A-C), for various cell types, determined by inductively coupled plasma–optical emission spectrometry (see Supplementary Material). The samples were filtered through 0.2-μm polyvinylidene fluoride filters (solid points, **A1–C1**) or 100-kD centrifugal filters (void points, **A2–C2**) before the ICP-OES analysis. The horizontal axis of each plot represents the reaction time (h). The error bar of each data point is the standard deviation of six analyses.

different. The more mobile free EPS could adsorb on oxide particle surfaces, and thus, modify particle surface charge (Table 1) and surface free radical concentrations. Capsular EPS provided bacterial cells with a physical barrier from the oxide particles and was also essential in biofilm production that offered microenvironments for heterogeneous growth of cell aggregates. Moreover, biofilm properties such as effective diffusion coefficient, charge distribution, and chemical composition determined the penetration of the oxide particles as well as the transport of nutrients and metabolites. Thus, the shielding effect of EPS against mineral toxicity depended on both chemical and physical mechanisms.

We recognize that the deletion of the *psl* gene cluster to create the Δ^{-}*psl* mutant bacteria might have affected genetic and biochemical pathways in the bacteria other than EPS and biofilm production. Our study accounted for these potential

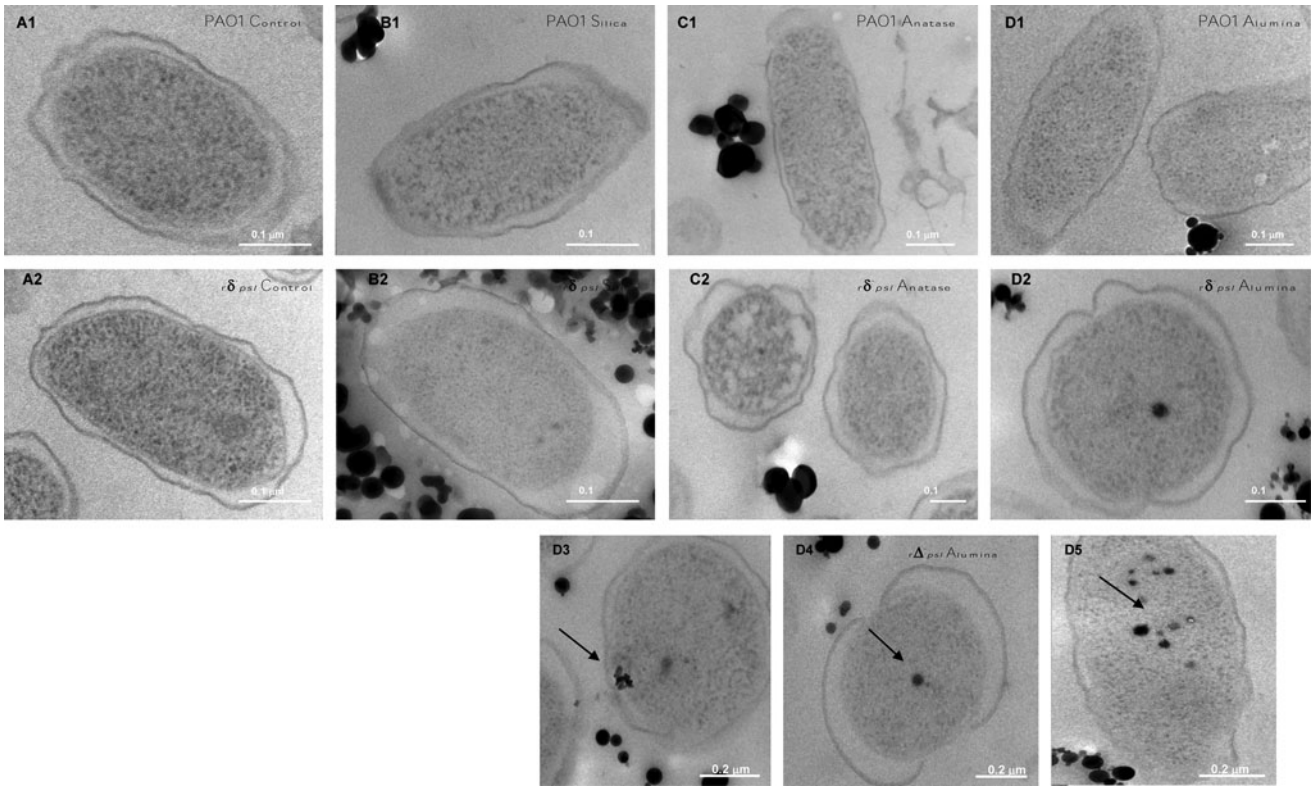

FIG. 5. High-resolution transmission electron micrographs of cells interacted with oxides for 7 h, processed by high-pressure freezing followed by fixation, substitution, embedding, and sectioning (see Supplementary Material). (**A1–D1**) PAO1 control and oxide samples; (**A2–D2**) rΔ^-*psl* control and oxide samples. Darker spots were observed only inside the rΔ^-*psl* cells reacted with γ-alumina. We interpret the dark spots as nanoparticles of γ-alumina that have penetrated the cytoplasm. (**D3–D5**) show additional microviews of the γ-alumina samples of rΔ^-*psl* cells. Scale bars are indicated on each image.

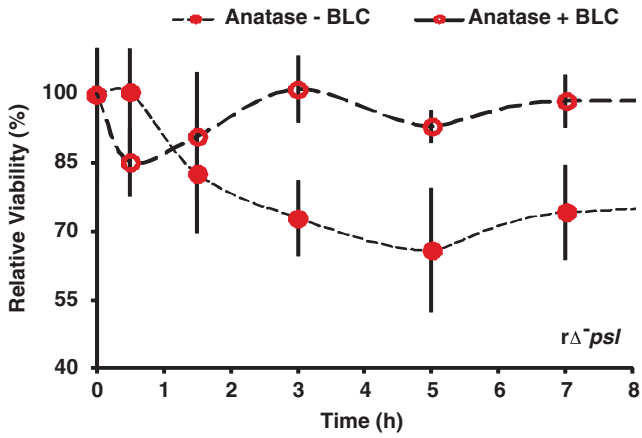

FIG. 6. Effect of bovine liver catalase (BLC), a scavenger of highly reactive oxygen species (hROS), on relative cell viability in the anatase + rΔ^-*psl* samples. The BLC-treated anatase (empty circles) showed no effect on the rΔ^-*psl* cells compared with the original, non-treated anatase (solid circles), indicating that formation of reactive oxygen species was the primary mechanism of anatase toxicity toward the EPS-devoid cells (also compare with Fig. 1).

effects, however, because we compared PAO1 with rPAO1 and Δ^-*psl* with rΔ^-*psl*. We used EPS-removed cells also because no mutant exists that is completely devoid of EPS. Preliminary results in our laboratory have also established similar effects for wild-type and biofilm-defective mutant strains of Gram-positive *Bacillus subtilis*.

4.2. Mineral toxicity mechanisms

Our study showed that not all minerals are benign or toxic; rather, their toxicity depended primarily on their chemical composition and surface chemistry, with toxicity increasing as $SiO_2 < \beta - TiO_2 < \gamma$-$Al_2O_3$. We considered several potential toxicity mechanisms for each oxide, including soluble metals, surface charge, particle size, and presence of hROS on the oxide surfaces.

4.2.1. Metal solubility versus nanoparticles. The binding of soluble metal(loid) ions to functional groups on bacterial EPS with subsequent formation of nanoparticulate mineral precipitates at cell surfaces has been proposed as a potential mechanism for shielding against soluble metal(loid) toxicity toward cells. Si solubility increased in the presence of EPS (Fig. 4). This result is consistent with reports that organic complexation of silica increased silica solubility and that bacterial colonization accelerated the dissolution rate of silica by surface complexation with organic species and by hydrolytic attack with enzymes and metabolites (Bennett, 1991;

Sahai and Tossell, 2001; Sahai, 2004). The increased soluble Si concentration, however, did not affect the cells, which indicates that Si was nontoxic at these concentrations.

The solubility of Ti was very low and did not change with filter size or with presence or absence of EPS, indicating that the anatase particles were mostly larger than 200 nm and that some other mechanism associated with TiO2 particle surface was responsible for its toxicity.

The toxicity of Al_2O_3 was affected by the filter size, which indicates that some fraction of the alumina particles existed as nanoparticles or as nano-oligomers < 200 nm in size. Intriguingly, an apparently smaller concentration of soluble Al was obtained for the rΔ^-*psl* cells compared to the PAO1 cells, which suggests that the former behaved as a sink for these particles, either through cellular internalization or by γ-alumina binding at the cell surface.

4.2.2. Intracellular versus extracellular nanoparticle toxicity. A fraction (<50 nm) of the positively charged alumina particles was found inside the rΔ^-*psl* cells (Fig. 5). Potential mechanisms for penetration of cells include introduction and enlargement of defects in the cell's outer membrane by γ-alumina particles, internalization of γ-alumina particles during cell division, and diffusion of Al oligomers through cell surface pores, with precipitation as nanoparticles within the cells (Nel *et al.,* 2009; Lin *et al.,* 2010; Verma and Stellacci, 2010). Interestingly, similar to our results for γ-alumina, the penetration of *P. aeruginosa* cells by insoluble Ag nanoparticles < 80 nm in size has been reported previously (Xu *et al.,* 2004), and the penetration mechanism was related with enlarged pores at the cell surface induced by higher levels of chloramphenicol production in the presence of Ag nanoparticles. Negatively charged native Ag nanoparticles were also less toxic than functionalized Ag nanoparticles of increasingly positive surface charge toward *Bacillus* strains, which have negative surface charge (Badawy *et al.,* 2011).

4.2.3. Surface charge. The outer membrane of gram-negative bacteria is predominantly constructed of polyanionic molecules (Nikaido and Vaara, 1985; Makin and Beveridge, 1996) and shows strong surface electronegativity. The negatively charged cell surface repelled the similarly charged amorphous silica and anatase particles in all the solutions (Table 1), so cell–particle contact for these two oxides was not intense and occurred mainly by mechanical rotations of the reactors (see Methods). The γ-alumina particle surfaces were positively charged in the rPAO1 and rΔ^-*psl* solutions. Electrostatic attraction between the rPAO1 or rΔ^-*psl* cells and the γ-alumina particles resulted in close cell–particle associations, which partly explains why the alumina nanoparticles and nano-oligomers < 0.2 μm were readily removed from the rΔ^-*psl* solution (Fig. 4C1, C2). HRTEM micrographs confirmed that γ-alumina particles < 50 nm had penetrated the rΔ^-*psl* cytoplasmic space (Fig. 5D2–D5). The surface charge of the γ-alumina particles was reversed to negative in the PAO1 solution (Table 1), likely due to the adsorption of EPS polyanionic ligands such as uronic acids and cell metabolites. Thus, EPS played a role in reversing surface charge of the particles, which then repelled PAO1 cells, in addition to providing a physical barrier to the particles.

The above interpretation for γ-alumina toxicity was supported by comparing the "soluble" Al data (Fig. 4C1) and the susceptibility of rΔ^-*psl* to oxides (Fig. 1). We noticed that after 7 h the concentration of alumina particles < 200 μm increased slightly, as did the potassium concentration (Fig. 4S). We attributed these results to the lysis of the Δ^-*psl* cells and the release of the internalized alumina particles and intracellular fluid. Thus, both size and surface charge were important particle properties in determining whether γ-alumina particles penetrated into cells.

The toxicity of aluminum is a well-known phenomenon (Martin, 1986; Exley and Birchall, 1992), and the intracellular toxicity of γ-alumina particles < 200 nm could have occurred via similar mechanisms as soluble aluminum complexes, including (1) noncovalent binding to specific biomolecular sites as on ATP or glycolytic enzymes, resulting in malfunctioning of the target molecules; (2) adsorption and depletion of cellular components such as phosphorus; or (3) inhibition of membrane transport proteins by interfering with the membrane potential (Exley and Birchall, 1992; Hamel and Appanna, 2001).

4.2.4. Is intracellular penetration (particle size < 50 nm) essential for particle toxicity? It is worthwhile to consider whether particle-size effects are required in mineral cytotoxicity. Particle size may be important in affecting cell viability for those minerals that are cytotoxic due to intracellular mechanisms, such as γ-alumina. The toxicity of anatase, however, must depend on another mechanism.

We observed high concentrations of hROS for anatase and, correspondingly, high susceptibility of rΔ^-*psl*. Surface-associated highly reactive oxygen species (hROS), such as H_2O_2 and •OH radicals, can be formed at high concentrations on the surface of anatase under aerobic conditions, because the band edge positions and gap energy allow effective excitation by a broad spectrum of UV light (Gratzel et al., 1983; Linsebigler et al., 1995). These hROS can catalyze peroxidation of phospholipids and degrade nucleic acids leading to cell lysis. The cytoxicity of titania due to surface hROS is well established in the literature (Kiraly *et al.,* 1997; Imlay and Linn, 1988; Gutteridge and Halliwell, 1990). The viability of rΔ^-*psl* cells was much greater in the presence of bovine liver catalase, which quenched the hROS, thus confirming our suggestion that the major cytotoxicity mechanism of anatase was by photocatalyzed hROS formation. The higher viability of PAO1 was attributed to the presence of EPS. We suggest that both capsular and free EPS could react with and quench the hROS, which would prevent the harmful oxidative effect of hROS from reaching the cells and, in addition, provide a physical barrier to the anatase particles.

The discussion above suggests that, for minerals that possess photocatalyzed surface free radicals, such as anatase, pyrite, olivines, and pyroxenes (Yen *et al.,* 2000; Schoonen *et al.,* 2010), the toxic effect can occur extracellularly, so larger, mm- or cm-sized crystals in rocks may still be cytotoxic to bacteria in contact. Thus, the dependence of toxicity on even a physical property such as particle size ultimately depends on the mineral chemistry.

4.3. Evolution of EPS

Several roles have been proposed for the evolution of EPS, including facilitating attachment to mineral surfaces,

protection against ultraviolet radiation, desiccation, and soluble metal toxicity, as well as providing a medium for concentrating quorum-sensing molecules and facilitating horizontal gene transfer. The results of this study indicate a previously unrecognized role for EPS in armoring against insoluble mineral toxicity. Cellular attachment to mineral surfaces at the bottom of tidal pools and other water bodies was probably an early adaptation that minimized damage by UV radiation relative to a planktonic mode of existence. Furthermore, the earliest cells were plausibly chemoautotrophic (Konhauser, 2007), and close contact with mineral surfaces would have been crucial for cell survival and function. EPS might, thus, have evolved to facilitate cell attachment to mineral surfaces, and the protective role against mineral-specific toxicity might have been a redundant function.

We have also shown previously that phospholipid vesicles, models for the earliest cells before the evolution of EPS, are ruptured in contact with specific oxide mineral surfaces, depending on the surface chemistry of the oxides (Xu *et al.*, 2009). It is then possible that a cell before the evolution of EPS could have been ruptured by mineral surfaces upon approaching a mineral in order to avoid direct UV damage or to facilitate metabolism. In this scenario, the evolution of EPS would have been an adaptation to shield against mineral toxicity, and attachment to mineral surfaces would have been simultaneously facilitated. In summary, regardless of the primary role for the evolution of EPS, the biofilm would have quickly provided multiple, redundant functions.

The oxide minerals and particular bacterial strains used in the present study, as well as the presence of free oxygen and oxygen reactive species, were model systems to illuminate the role of EPS as a shield. We do not mean to imply that these specific oxides or bacteria (e.g., aerobic, gram-negative, heterotrophic, etc.) and oxygen free radicals were necessarily present on early Earth. Nonetheless, oxyhydroxides, clays, and other silicates or carbonate minerals may have dominated on early Earth, depending on atmospheric CO_2 levels (Schoonen *et al.*, 2004). Also, some concentration of oxygen free radicals as well as plentiful free radicals from reactions involving CO_2, NO_2, SO_2 generated by UV radiation, lightening, and impacts could have existed.

In addition, the formation of biofilms is widespread among both anaerobic and aerobic microorganisms, gram-positive and gram-negative. Moreover, the EPS-removed rPAO1 and rΔ^-*psl* cells were the cell types that most clearly demonstrated that EPS acts as armor against toxic minerals and that EPS production can be stimulated by these toxic minerals. These EPS-removed cells were exposed to nutrient-limited conditions that were likely more closely representative of early Earth conditions than the enriched media for the PAO1 and Δ^-*psl* cell cultures.

4.4. Implications

Both geological and phylogenetic records show that biofilm formation is an ancient and integral component of prokaryotic life. Putative biofilms have been identified in the 3.3–3.4 Ga South Africa Kornberg Formation (Westall *et al.*, 2001) based on subspherical morphological features, and filamentous forms reminiscent of modern cyanobacteria have been identified in the 3.2 Ga Pilbara Craton of Western Australia (Rasmussen, 2000). The biofilm matrix is also a characteristic of prokaryotic "living fossils," the Korarchaeota and Aquificales, extant lineages of the most ancient Bacteria and Archaea (Reysenbach *et al.*, 2000; Jahnke *et al.*, 2001). In the context of evolution and adaptation, biofilms likely evolved as primitive homeostasis against fluctuating and extreme geochemical conditions on early Earth. Whatever the original role of EPS, biofilms could have quickly provided redundant functions in protecting normal cell functions from environmental extremes, including particulate mineral toxicity.

Acknowledgments

This research was financially supported by the NSF career award 0346689, NASA Astrobiology Institute Director's Discretionary Fund 2008 grant, and by University of Akron "start-up" funds to Nita Sahai. Jie Xu was supported partially by the Weeks Graduate Fellowship through the Department of Geoscience, University of Wisconsin-Madison. We thank Prof. M. Parsek and Prof. Y. Liu for providing the bacterial strains, Prof. E. Roden for use of the epi-fluorescence microscope, and Dr. S. Cheng and Dr. E. Shelobolina for technical assistance and helpful discussions, which significantly improved the manuscript.

Disclosure Statement

No competing financial interests exist.

References

Badawy, A.M., Silva, R.G., Morris, B., Scheckel, K.G., Suidan, M.T., and Tolaymat, T.M. (2011) Surface charge-dependent toxicity of silver nanoparticles. *Environ Sci Technol* 45:283–287.

Banfield, J.F. and Hamers, R.J. (1997) Processes at minerals and surfaces with relevance to microorganisms and prebiotic synthesis. In *Geomicrobiology: Interactions between Microbes and Minerals*, edited by J.F. Banfield, and K.H. Nealson, American Mineralogical Society, Washington, D.C., pp 81122.

Bennett, P.C. (1991) Quartz dissolution in organic-rich aqueous systems. *Geochim Cosmochim Acta* 55:1781–1797.

Beveridge, T.J., Makin, S.A., Kadurugamuwa, J.L., and Li, Z.S. (1997) Interactions between biofilms and the environment. *FEMS Microbiol Rev* 20:291–303.

Brayner, R., Ferrari-Iliou, R., Brivois, N., Djediat, S., Benedetti, M.F., and Fievet, F. (2006) Toxicological impact studies based on Escherichia coli bacteria in ultrafine ZnO nanoparticles colloidal medium. *Nano Lett* 6:866–870.

Brown, G.E., Henrich, V.E., Casey, W.H., Clark, D.L., Eggleston, C., Felmy, A., Goodman, D.W., Gratzel, M., Maciel, G., and McCarthy, M.I. (1999) Metal oxide surfaces and their interactions with aqueous solutions and microbial organisms. *Chem Rev* 99:77–174.

Cairns-Smith, A.G. (1982) *Genetic takeover and the mineral origins of life,* Cambridge University Press, Cambridge.

Cohn, C.A., Pedigo, C.E., Hylton, S.N., Simon, S.R., and Schoonen, M.A.A. (2009) Evaluating the use of 3′-(p-Aminophenyl) fluorescein for determining the formation of highly reactive oxygen species in particle suspensions. *Geochem T* 10:1–9.

Costerton, J.W., Lewandowski, Z., Caldwell, D.E., Korber, D.R., and Lappinscott H.M. (1995) Microbial biofilms. *Annu Rev Microbiol* 49:711–745.

Exley, C. and Birchall, J.D. (1992) The cellular toxicity of aluminum. *J Theor Biol* 159:83–98.

Ferris, J.P., Hill, A.R., Liu, R.H., and Orgel, L.E. (1996) Synthesis of long prebiotic oligomers on mineral surfaces. *Nature* 381:59–61.

Geesey, G.G., Jang, L., Jolley, J.G., Hankins, M.R., Iwaoka, T., and Griffiths, P.R. (1988) Binding of metal-ions by extracellular polymers of biofilm bacteria. *Water Sci Technol* 20:161–165.

Gogniat, G., Thyssen, M., Denis, M., Pulgarin, C., and Dukan, S. (2006) The bactericidal effect of TiO_2 photocatalysis involves adsorption onto catalyst and the loss of membrane integrity. *FEMS Microbiol Lett* 258:18–24.

Gratzel, M. (1983) *Energy resources through photochemistry and catalysis*, Academic Press, New York/London.

Gutteridge, J.M.C. and Halliwell, B. (1990) The measurement and mechanism of lipid-peroxidation in biological-systems. *Trends Biochem Sci* 15:129–135.

Hall-Stoodley, L., Costerton, J.W., and Stoodley, P. (2004) Bacterial biofilms: From the natural environment to infectious diseases. *Nat Rev Microbiol* 2:95–108.

Hamel, R.D. and Appanna, V.D. (2001) Modulation of TCA cycle enzymes and aluminum stress in Pseudomonas fluorescens. *J Inorg Biochem* 87:1–8.

Harrison, J.J., Ceri, H., and Turner, R.J. (2007) Multimetal resistance and tolerance in microbial biofilms. *Nat Rev Microbiol* 5:928–938.

Hochella, M.F., Lower, S.K., Maurice, P.A., Penn, R.L., Sahai, N., Sparks, D.L., and Twining, B.S. (2008) Nanominerals, mineral nanoparticles, and earth systems. *Science* 319:1631–1635.

Imlay, J.A. and Linn, S. (1988) DNA damage and oxygen radical toxicity. *Science* 240:1302–1309.

Jahnke, L.L., Eder, W., Huber, R., Hope, J.M., Hinrichs, K.U., Hayes, J.M., Des Marais, D.J., Cady, S.L., and Summons, R.E. (2001) Signature lipids and stable carbon isotope analyses of octopus spring hyperthermophilic communities compared with those of *Aquificales* representatives. *Appl Environ Microbiol* 67:5179–5189.

Kiraly, Z., ElZahaby, H.M., and Klement, Z. (1997) Role of extracellular polysaccharide (EPS) slime of plant pathogenic bacteria in protecting cells to reactive oxygen species. *J Phytopathol* 145:59–68.

Konhauser, K. (2007) *Introduction to geomicrobiology*, Blackwell Publications, Malden, MA.

Lin, J.Q., Zhang, H.W., Chen, Z., and Zheng, Y.G. (2010) Penetration of lipid membranes by gold nanoparticles:insights into cellular uptake, cytotoxicity, and their relationship. *Acs Nano* 4:5421–5429.

Linsebigler, A.L., Lu, G.Q., and Yates, J.T. (1995) Photocatalysis on TiO_2 surfaces – principles, mechanisms, and selected results. *Chem Rev* 95:735–758.

Makin, S.A. and Beveridge, T.J. (1996) The influence of A-band and B-band lipopolysaccharide on the surface characteristics and adhesion of Pseudomonas aeruginosa to surfaces. *Microbiol-UK* 142:299–307.

Martin, R.B. (1986) The chemistry of aluminum as related to biology and medicine. *Clin Chem* 32:1797–1806.

Metzger, U., Lankes, U., Fischpera, K., and Frimmel, F.H. (2009) The concentration of polysaccharides and proteins in EPS of *Pseudomonas putida* and *Aureobasidum pullulans* as revealed by C-13 CPMAS NMR spectroscopy. *Appl Microbiol Biotechnol* 85:197–206.

Miller, M.B. and Bassler, B.L. (2001) Quorum sensing in bacteria. *Annu Rev Microbiol* 55:165–199.

Nealson, K.H., Tebo, B.M., and Rosson, R.A. (1988) Occurrence and mechanisms of microbial oxidation of manganese. *Adv Appl Microbiol* 33:279–318.

Nel, A.E., Madler, L., Velegol, D., Xia, T., Hoek, E.M.V., Somasundaran, P., Klaessig, F., Castranova, V., and Thompson, M. (2009) Understanding biophysicochemical interactions at the nano-bio interface. *Nat Mater* 8:543–557.

Neu, T.R., Swerhone, G.D.W., and Lawrence, J.R. (2001) Assessment of lectin-binding analysis for in situ detection of glycoconjugates in biofilm systems. *Microbiol-SGM* 147:299–313.

Nikaido, H. and Vaara, M. (1985) Molecular-basis of bacterial outer-membrane permeability. *Microbiol Rev* 49:1–32.

O'Toole, G., Kaplan, H.B., and Kolter, R. (2000) Biofilm formation as microbial development. *Annu Rev Microbiol* 54:49–79.

Omoike, A. and Chorover, J. (2004) Spectroscopic study of extracellular polymeric substances from Bacillus subtilis: Aqueous chemistry and adsorption effects. *Biomacromolecules* 5:1219–1230.

Overhage, J., Schemionek, M., Webb, J.S., and Rehm, B.H.A. (2005) Expression of the psl operon in *Pseudomonas aeruginosa* PAO1 biofilms: *PslA* performs an essential function in biofilm formation. *Appl Environ Microbiol* 71:4407–4413.

Rasmussen, B. (2000) Filamentous microfossils in a 3,235-million-year-old volcanogenic massive sulphide deposit. *Nature* 405:676–679.

Reysenbach, A.L., Ehringer, H., and Hershberger, K. (2000) Microbial diversity at 83°C in Calcite Springs, Yellowstone National Park: another environment where the *Aquificales* and "*Korarchaeota*" coexist. *Extremophiles* 4:61–67.

Sahai, N. and Tossell, J.A. (2001) Formation energies and NMR chemical shifts calculated for putative serine-silicate complexes for silica biomineralization. *Geochim Cosmochim Acta* 65:2043–2053.

Sahai, N. (2004) Calculation of Si-29 NMR shifts of silicate complexes with carbohydrates, amino acids, and carboxylic acids: potential role in biological silica utilization. *Geochim Cosmochim Acta* 68:227–237.

Schoonen, M.A.A., Cohn, C.A., Roemer, E., Laffers, R., Simon, S.R., and O'Riordan, T. (2006) Mineral-induced formation of reactive oxygen species. In *Medical Mineralogy*, edited by N. Sahai and M.A.A. Schoonen, American Mineralogical Society, Washington, D.C., pp 179–211.

Schoonen, M.A.A., Smirnov, A., and Cohn, C. (2004) A perspective on the role of minerals in prebiotic synthesis. *Ambio* 33:539–551.

Schoonen, M.A.A., Harrington, A.D., Laffers, R., and Strongin, D.R. (2010) Role of hydrogen peroxide and hydroxyl radical in pyrite oxidation by molecular oxygen. *Geochim Cosmochim Acta* 74:4971–4987.

Stanley, N.R. and Lazazzera, B.A. (2004) Environmental signals and regulatory pathways that influence biofilm formation. *Mol Microbiol* 52:917–924.

Sutherland, I.W. (2001) Biofilm exopolysaccharides: a strong and sticky framework. *Microbiol-UK* 147:3–9.

Tebo, B.M., Bargar, J.R., Clement, B.G., Dick, G.J., Murray, K.J., Parker, D., Verity, R., and Webb, S.M. (2004) Biogenic manganese oxides:properties and mechanisms of formation. *Annu Rev Earth Planet Sci* 32:287–328.

VanCappellen, P. and Wang, Y.F. (1996) Cycling of iron and manganese in surface sediments: A general theory for the coupled transport and reaction of carbon, oxygen, nitrogen, sulfur, iron, and manganese. *Am J Sci* 296: 197–243.

Verma, A. and Stellacci, F. (2010) Effect of surface properties on nanoparticle–cell interactions. *Small* 6:12–21.

Wachtershauser, G. (1988) Before enzymes and templates – theory of surface metabolism. *Microbiol Rev* 52:452–484.

Weber, K.A., Achenbach, L.A., and Coates, J.D. (2006) Microorganisms pumping iron: anaerobic microbial iron oxidation and reduction. *Nat Rev Microbiol* 4:752–764.

Westall, F., de Wit, M.J., Dann, J., van der Gaast, S., de Ronde, C.E.J., and Gerneke, D. (2001) Early archean fossil bacteria and biofilms in hydrothermally influenced sediments from the Barberton greenstone belt, South Africa. *Precambrian Res* 106:93–116.

Xu, J., Stevens, M.J., Oleson, T.A., Last, J.A., and Sahai, N. (2009) Role of oxide surface chemistry and phospholipid phase on adsorption and self-assembly: isotherms and atomic force microscopy. *J Phys Chem C* 113:2187–2196.

Xu, X.H.N., Brownlow, W.J., Kyriacou, S.V., Wan, Q., and Viola, J.J. (2004) Real-time probing of membrane transport in living microbial cells using single nanoparticle optics and living cell imaging. *Biochemistry* 43:10400–10413.

Yen, A.S., Kim, S.S., Hecht, M.H., Frant, M.S., and Murray, B. (2000) Evidence that the reactivity of the martian soil is due to superoxide ions. *Science* 289:1909–1912.

Address correspondence to:
Nita Sahai
170 University Avenue
Department of Polymer Science and
NASA Astrobiology Institute
University of Akron
Akron, OH 44313-3909

E-mail: sahai@uakron.edu

or

Jie Xu
Department of Chemistry
2029 G street Northwest
George Washington Unviersity
Washington, DC 20052

E-mail: jxu@gwu.edu